IIETA International Information and Engineering Technology Association
Advancing the World of Information and Engineering

Instrumentation Mesure Métrologie
Vol. 25, No. 3, June, 2026, pp. 103-112
Journal homepage: http://iieta.org/journals/i2m

Identification of Optimal Adaptive Neuro-Fuzzy Inference System Input Variables for Daily Global Solar Radiation Prediction in Adrar, Algeria

Abdeldjbar Babahadj[1*], Fateh Ferroudji[1], Mebrouk Bellaoui[1], Kada Bouchouicha[2]

[1] Unité de Recherche en Energie Renouvelables en Milieu Saharien (URERMS), Centre de Développement des Energies Renouvelables (CDER), Adrar 01000, Algeria
[2] Centre de Développement des Energies Renouvelables (CDER), Bouzaréah 16340, Algeria

Corresponding Author Email: babahadj1981@gmail.com

https://doi.org/10.18280/i2m.250301

Received: 2 February 2026
Revised: 3 May 2026
Accepted: 11 May 2026
Available online: 26 June 2026

Keywords:
solar radiation, daily global, adaptive neuro-fuzzy inference system, Adrar city, Algerian Big South

ABSTRACT

Estimating the amount of solar radiation (SR) from the sun at a given site is very significant in evaluating the potential of energy to reliably forecast the potential and performance behavior of solar power applications. This study aimed to use an intelligent optimization scheme based on the adaptive neuro-fuzzy inference system (ANFIS) technique to identify the most critical parameters for predicting the daily horizontal global SR. The data was collected from a measured meteorological station in Adrar city, Algeria, in the period of 2014 to 2018. Different combinations of extraterrestrial irradiation (H_0), maximum, average, and minimum of air temperature (T_{max}, T_{avg}, and T_{min}), relative humidity (R_h), the wind speed (W_s), and water vapor pressure (V_P) were considered as influential input parameters in the developed model. 75% of the data was applied to train, test, and validate the ANFIS model. The results attained indicate that the combination of H_0 and T_{min} is the most suitable input combination, achieving a Global Performance Indicato (GPI) value of 3.79 (with higher GPI values indicating better performance) with Correlation Coefficient (R) = 0.9451, Root Mean Square Error (RMSE) = 0.5255, Mean Percentage Error (MPE) = 6.35, and Mean Absolute Bias Error (MABE) = 0.313 in the training phase. In the testing R = 0.9360, RMSE = 0.5728, MPE = 6.114 and MABE = 0.296. This finding underscores the model's efficiency and robustness. Consequently, the proposed ANFIS model provides a practical and reliable tool for solar resource assessment, system sizing, and grid integration planning in the Adrar region and similar arid environments.

1. INTRODUCTION

Emphasis on renewable energy in the last few years has resulted in a significant increase in investments in the global energy system. Among all these energies, solar energy is considered the prime candidate among renewable energies. Solar energy has many practical applications, such as photovoltaic conversion systems and thermal conversion systems. The design, development, and performance of these applications are highly dependent on the solar radiation (SR) data for any geographical location [1, 2]. Hence, it is a primary requirement for evaluating the availability of SR in the designated site of interest [3].

Over the years, the challenges associated with directly measuring SR, the solar researchers have developed many methods for estimating SR using different meteorological, geometrical and astronomical parameters. The most common among them are the satellite-derived [4-6], stochastic algorithm [7] and empirical models [8, 9]. The first and second models are new and may be subject to shortage and model validation of available data, respectively. The empirical models are more commonly used in the agriculture and hydrology studies, since they involve a general practice based on other available meteorological parameters. The most important of these parameters are sunshine durations, air temperature, wind speed, air pressure, relative humidity, and cloudiness [10]. The empirical models (or soft computing) include artificial neural network (ANN), genetic algorithms (GAs), support vector machine (SVM), and adaptive neuro-fuzzy inference system (ANFIS), which have received much attention because they are appropriate to model dynamic and nonlinear systems [10, 11].

In recent years, some soft computing models have been extensively utilized worldwide for estimating global SR; among them, ANFIS and ANN are the most commonly preferred. Numerous studies have tried to enhance SR prediction models by improving only the ANFIS model. Mellit et al. [12] used the ANFIS model to predict global SR in Algeria using air temperature and sunshine duration, and showed that the ANFIS model demonstrates suitability for cases where no recorded total daily SR data is available (missing data). Sumithira and Nirmal Kumar [13] performed a study comparing ANFIS with other soft computing models in order to predict global SR in Tamil Nadu, India. The results showed that the ANFIS model provides better results than other models and is compatible with any geographic region

with varying meteorological conditions. Güçlü et al. [14] analyzed SR estimation for three cities (Adana, Antakya, and Silifke) in Turkey using both ANFIS and Angström-Prescott models and found that the ANFIS model demonstrates superior estimation capacity compared to other models. Olatomiwa et al. [15] developed an ANFIS model for simulating SR in Iseyin, Nigeria and found that the ANFIS model is an effective technique in estimating SR for practical applications. Mohammadi et al. [16] employed ANFIS technique to determine the most relevant parameters in order to estimate the daily global SR in three cities (Isfahan, Kerman and Tabas), located in Iran. The results indicated that the optimal input combinations vary among the three cities because of differences in their characteristics of SR and climate conditions. Quej et al. [10] examined the performance of ANN, SVM, and ANFIS techniques to predict horizontal global SR using recorded meteorological variables in the Yucatán Peninsula, located in Mexico. The results showed that the SVM technique has better performance than the other techniques. Zou et al. [17] conducted a study to predict daily global solar irradiance in China using the ANFIS technique. The results indicated that the ANFIS provides a superior performance relative to the other models in predicting. Halabi et al. [18] proposed a hybrid ANFIS model and a standalone ANFIS to predict monthly global SR in the Kuala Terengganu region, Malaysia. They found that ANFIS integrated with the particle swarm optimization model had superior performance to the other soft computing models. Alsharif and Younes [19] used ANFIS to forecast and evaluate to predict the average monthly SR in Seoul city, Republic of Korea. The results indicated variation independent of location (with an average normalized root mean square error (NRMSE) of around 1%). However, the effectiveness of this system is limited by the effect of diverse meteorological conditions, such as clouds, that influence both the duration and intensity of the SR. Tao et al. [20] proposed a novel model by hybridization of ANFIS with two metaheuristic optimization algorithms for the prediction of global SR in various locations of North Dakota, USA. The results demonstrated a significant enhancement in the ANFIS model performance achieved via the optimization of its internal parameters. Fraihat et al. [21] studied the influence of 24 meteorological parameters on predicting SR in the west-central region of Jordan using ANFIS and long short-term memory (LSTM) models. The results showed that the ANFIS model provides better results than the LSTM model when the parameter correlation with SR is high. Geshnigani et al. [22] used seven different artificial intelligence models, such as ANFIS and ANN, for estimating daily SR at eleven meteorological stations in Illinois, located in the USA. They found that growing the number of inputs significantly enhances the performance of the ANFIS model using evolutionary algorithms. Anupong et al. [23] estimated the effectiveness of the Wavelet Artificial Neural Network (WANN), Wavelet Support Vector Machine (WSVM), and ANFIS models in estimating the amount of solar energy in two stations (Wasit and Dhi Qar), located in Iraq. The results demonstrated that all three models predict the result well, and the ANFIS result was less accurate than the other two models.

Among intelligent forecasting methods, ANFIS has carved out a strong niche by combining the learning flexibility of neural networks with fuzzy logic's ability to handle uncertainty and generate interpretable rules. It is particularly effective at modeling the complex relationships between solar irradiance and key meteorological variables such as sunshine duration, temperature, and humidity. Recent studies provide compelling evidence of ANFIS's performance in harsh, sun-drenched environments. Halima et al. [24] showed that in southern Algeria, ANFIS outperformed GA-ANN hybrids and standalone ANN models for daily SR forecasting, achieving R = 0.9374 and MAPE ≈ 7.8%, especially under dusty, challenging conditions. Similarly, Nafa et al. [25] demonstrated that ANFIS could act as a virtual sensor, estimating irradiance from PV module voltages and currents with near-perfect accuracy ($R^2 \approx 0.99999$). Field trials in the UAE confirmed ANFIS-based power forecasts could reach $R^2 \approx 0.997$ for grid-connected PV plants, even under extreme heat and sand exposure [26]. These results highlight the robustness and adaptability of ANFIS across diverse desert climates and operational conditions.

Several studies have investigated SR prediction in the Algerian Big South using empirical models [27-29]. However, to our knowledge, no study has specifically addressed the selection of optimal input combinations for daily global SR estimation in the southwest of Algeria (Adrar city) using the ANFIS technique. To fill this gap, the present study employs ANFIS to identify the most significant parameters influencing daily horizontal global SR in dry desert conditions.

For the case study, Adrar city, located in the southwest of Algeria, was selected due to its hyper-arid climate and high solar potential. The analysis is based on five years of measured meteorological data (2014–2018) from the only available local meteorological station. This dataset provides sufficient coverage to capture typical seasonal and annual variability while allowing for robust modeling of SR dynamics in this region.

2. METHODOLOGY

2.1 Study area

This study selected a station in the Adrar province of Algeria. Figure 1 displays the geographical situation of this province. Adrar province, with geographical coordinates (latitude 27.88° N, longitude 0.28° W, and altitude 263 m), is situated in the extreme southwest of Algeria. It represents the second largest city, which occupies about 427,968 km² (1/5 of Algeria's territory). Based on Köppen-Geiger climate classification [30], the Adrar region has a hot desert climate BWh. This climate is largely characterized by long and hot summers (maximum annual ambient temperature ranges from 20 to 46 °C), short mild winters, low humidity rate (between 12 and 38%), and deficient precipitation almost all year round [27]. Additionally, the Adrar region is characterized by extremely high SR, with the global SR in winter and summer ranging from 5.47 to 7.86 kWh/m² [28, 29]. Due to all these reasons, it strongly favors the solar application and other renewable energy types (wind, thermal, etc.).

2.2 Data

In this current study, the Metrological station (New Energy Algeria, NEAL) was exploited for measuring solar irradiation values. The station (see Figure 2) was installed at Adrar, Algeria, specifically at the Research Unit in Renewable Energy in Saharan Medium (URER-MS, CDER). The database collection represents 5 years of data, from January 2014 to December 2018, recorded at 10-min intervals using

Kipp & Zonen CMP21 pyranometers. In addition, the station measures the daily meteorological parameters such as relative humidity, maximum and minimum ambient temperature, air pressure, speed and direction of the wind [29].

Technical specifications of the solar instrument used and the meteorological parameter sensors are listed in Table 1 [31].

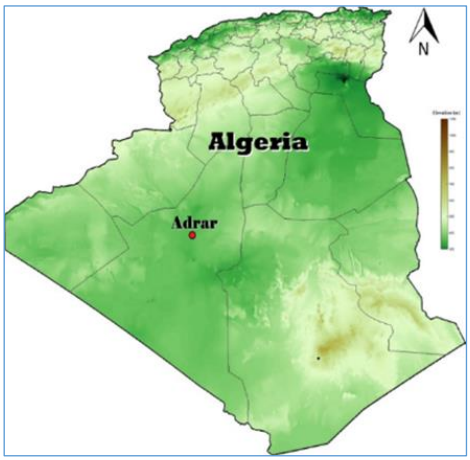

Figure 1. Algeria map showing the geographical location of Adrar province

Table 1. Technical characteristics of the utilized solar instrument

Sensor	Kipp & Zonen CMP21
Maximum operational irradiance	4000 W/m^2
Spectral range	270 to 3000 nm
Sensitivity	7 to 14 µV/W/m^2
Directional response	<10 W/m^2
Non-stability (Change/year)	<0.5%
Temperature response	<1% (−20 °C to +50 °C)
Response time	<5 s
Non-linearity	<0.2%
Operating and storage temperature range	−40 °C to +80 °C

Figure 2. Image of the meteorological station installed at URER-MS, Adrar

The global SR measurements are treated using simple quality control procedures described in detail by Bailek et al. [31]. Figure 3 shows the distribution of solar irradiance during a one-year period, which refers to a 5-year average of the measurements (from 2014 to 2018). According to Mohammadi et al. [16], a four-year dataset is sufficient for developing a robust ANFIS model. Therefore, this study uses the 2014–2018 period, representing the most complete and reliable dataset available for the Adrar region. These five years capture typical seasonal and yearly variations in this hyper-arid climate, making them sufficient for developing a robust ANFIS model. Using this contiguous dataset also accounts for the practical limitations of data availability in the region while ensuring representative coverage for model training and validation.

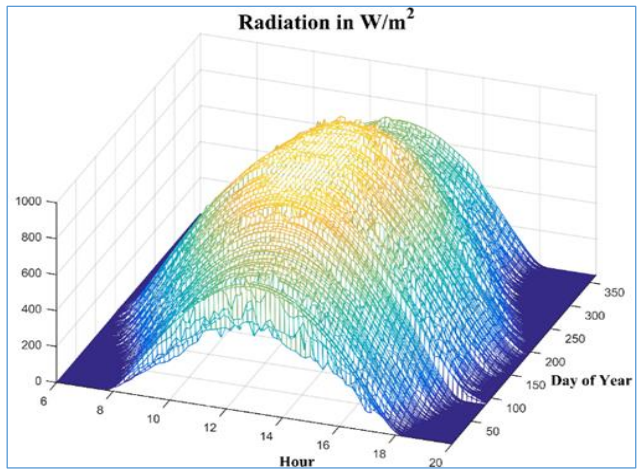

Figure 3. Variation of solar radiation (SR) in the Research Unit in Renewable Energy in Saharan Medium (URER-MS) site for the annual period

2.3 Adaptive neuro-fuzzy inference system

The ANFIS model, proposed by Jang [32], represents an innovative and simplified data-driven approach for determining the behavior of complex dynamical systems that are imprecisely defined. It combines the advantages of two machine learning methods (Fuzzy system and ANN). The ANFIS model has been commonly utilized in different domains for predicting temperature [33], rainfall [34], evaporation [35], runoff [36], etc. The ANFIS model is successful in predicting the SR and it is adaptable for designing standalone systems in various applications of solar energy [13]. The ANFIS under consideration utilizes the first-order Takagi–Sugeno-type fuzzy model [37].

The common rule set consists of two fuzzy if-then rules, which are as follows:

Rule 1: If x is A_1, y is B_1, then

$$F_1 = c11x + c12y + c1 \quad (1)$$

Rule 2: If x is A_2, y is B_2, then

$$F_2 = c21x + c22y + c2 \quad (2)$$

where, x and y are the inputs in the crisp set; A_1, A_2, B_1, B_2 are the linguistic labels F_1 and F_2 are the output fuzzy membership functions $c = \lfloor c_{ij} \rfloor,\ i,j = 1,2$ is the consequent parameter.

The ANFIS model structure (Figure 4) involves 2 input node layers, of which are base nodes, intermediate nodes, result nodes and output sssnodes.

Layer 1 (Fuzzy layer): Every node i in this layer is a square node with a node function:

$$O_{l,i} = \mu_{A,i}(x), \text{ for } i = 1, 2, \ldots, n \quad (3)$$

where, $\mu_{A,i}(x)$ represents the fuzzy concept A_i. The typical choice for the membership function is a bell-shaped curve with values ranging from 0 to 1. Examples of bell-shaped membership functions include the generalized bell function and the Gaussian function.

$$\mu_{A,i}(x) = \frac{1}{1 + \left[\left(\frac{x - c_i}{a}\right)^2\right]^{b_i}} \quad (4)$$

$$\mu_{A,i}(x) = exp\left[-\left(\frac{x - c_i}{a}\right)^2\right] \quad (5)$$

where, $\{a_i, b_i, c_i\}$ (or $\{a_i, c_i\}$ in the latter case) is known as the premise parameter set. For the current application, the generalized bell function type is selected for the membership functions.

Layer 2 (Product layer): This layer has a circular shape labeled with Π in Figure 4. In this layer, the nodes carry out a multiplication operation on the incoming signals and produce the resulting product here:

$$\bar{w}_i = \mu_{A,i}(x) \times \mu_{B,i}(y) \text{ for } i = 1, 2 \quad (6)$$

Layer 3 (Normalized layer): In this layer, the node is denoted with N. The i^{th} node calculates the ratio of the normalized firing strength (which is known as the quantity, $\bar{w}_i$) of the ith rule to the sum of the firing strength of all the rules:

$$o_1^3 = \bar{w}_i = \frac{w_i}{w_1 + w_2} \text{ for } i = 1, 2 \quad (7)$$

where, the o_1^3 is the output of the Layer 3.

Layer 4 (De-fuzzy layer): In this layer, the nodes are indicated with a square shape and they are associated with a specific node function as follows:

$$o_1^4 = \overline{w_i} f_i = \overline{w_i}(p_i x + q_i y + r_i) \text{ for } i = 1, 2 \quad (8)$$

where, $\overline{w_i}$ is the output of Layer 3 and $\{p_i, q_i, r_i\}$ are the coefficients in the Sugeno inference system represent the parameters of a linear combination. These parameters within this layer are commonly referred to as the consequent parameters (result parameters).

Layer 5 (Total output layer): The fixed node with label Σ, which determines the overall output value by summing all input signals from Layer 4, is the only node in this layer:

$$\begin{aligned} o_1^5 &= \sum_i \overline{w_i} f_i = \frac{\sum_i W_i f_i}{\sum_i W_i} \\ &= Overalloutput \\ f_i &= \\ &(\overline{w_1} x) p_1 + (\overline{w_1} y) q_1 + \left(\overline{w_1}\right) r_1 \\ &+ \left(\overline{w_2} x\right) p_2 + \left(\overline{w_2} y\right) q_2 + (\overline{w_2}) r_2 \end{aligned} \quad (9)$$

The learning method applied by ANFIS is a hybrid learning algorithm that consists of two passes: the forward pass and the backward pass. During the forward pass (1st pass), the premise parameters are kept fixed, and the consequent parameters are estimated using the least squares method. In the backward pass (2nd pass), the consequent parameters are fixed, and the premise parameters are updated using gradient descent, which is a supervised learning approach. The training and evaluation of the Fuzzy Inference System (FIS) in MATLAB are carried out throughout the entire process. To accomplish this, four cases involving 2, 3, 4, and 5 input parameters are examined and evaluated.

Figure 4 demonstrates the structure of a two-layer ANFIS model.

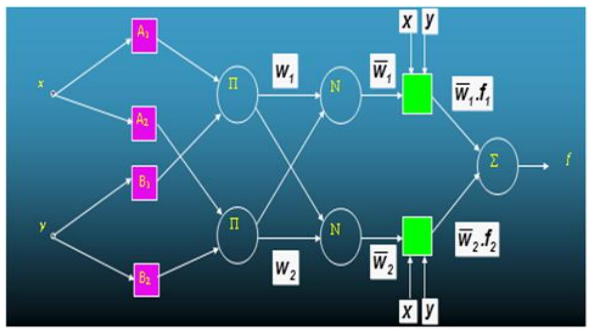

Figure 4. The architecture of the adaptive neuro-fuzzy inference system (ANFIS) model

2.4 Evaluation metrics

The performance of the developed ANFIS models was rigorously evaluated using a suite of statistical metrics to assess different aspects of prediction accuracy. The Correlation Coefficient (R), Root Mean Square Error (RMSE), Mean Percentage Error (MPE) and Mean Absolute Bias Error (MABE) [32].

$$R = \frac{\sum_{i=1}^{N}\left(H_{est}^{(i)} - \bar{H}_{est}\right)\left(H_{Meas}^{(i)} - \bar{H}_{Meas}\right)}{\sqrt{\sum_{i=1}^{N}\left(H_{est}^{(i)} - \bar{H}_{est}\right)^2 \sum_{i=1}^{N}\left(H_{Meas}^{(i)} - \bar{H}_{Meas}\right)^2}} \quad (10)$$

$$RMSE = \sqrt{\frac{1}{N}\sum_{i=1}^{N}\left(H_{est}^{(i)} - H_{Meas}^{(i)}\right)^2} \quad (11)$$

$$MPE = \frac{100}{N}\sum_{i=1}^{N}\frac{\left(H_{est}^{(i)} - H_{Meas}^{(i)}\right)}{H_{Meas}^{(i)}} \quad (12)$$

$$MABE = \frac{1}{N}\sum_{i=1}^{N}\left|H_{est}^{(i)} - H_{Meas}^{(i)}\right| \quad (13)$$

where, N is the total number of data points, $H_{est}^{(i)}$ and $H_{Meas}^{(i)}$ are the estimated and observed daily SR values, respectively.

Preliminary comparison of all models revealed that many could be excluded from final consideration due to high MPE, RMSE and MABE values or a low R magnitude. However, to objectively determine the single best model for predicting global SR from this large set, a composite Global Performance Indicator (GPI) was used, as defined by this study [28]:

$$GPI_i = \sum_j \alpha_J \left(\bar{z}_i - \bar{z}_{i,j} \right) \quad (14)$$

where, a_J equals 1 for the four indicators (MPE, RMSE) and for R equal to -1. $\bar{z}_j$ is the median of the scaled values of indicator j, $\bar{z}_{i,j}$ is the scaled value of indicator j for the i^{th} model.

3. RESULTS AND DISCUSSION

In this current study, the ANFIS learning technique was used to evaluate the influence of seven influential input parameters of H_0, T_{min}, T_{avg}, and T_{max}, R_h, W_s, and V_p on the prediction of daily horizontal global SR in the southwest of Algeria (Adrar city) and then find the best-input parameter sets. The collected data were divided into two sets: 75% of the data sets were employed for training and the subsequent 25% served for testing.

An overall search was executed for various possible combinations of the used input parameters of the input parameters to select the best combination of 2 or 3 inputs. In order to attain this objective, several ANFIS models were built and trained for a single epoch separately and respectively. Next, the performance achieved was reported on the basis of each combination. Five statistical parameters of MABE, MAPE, RMSE, R, and GPI were utilized as reliable indicators for evaluating the global SR prediction accuracy. The set of inputs that generates the highest GPI must be regarded as the most relevant regarding outcome (i.e., daily global SR prediction). The selection of the most important parameters was conducted for four cases. Various possible parameter combinations of two, three, four, and five input elements were considered, respectively. Then, we determined both the optimal and least sets of inputs. The results obtained are presented and discussed in the upcoming sub-sections.

3.1 Case 1: Parameter selection for a combination of 2 inputs

For the first case, two parameters were considered as input. For this objective, the 21 possible combinations of inputs (21 ANFIS models) were developed and analyzed. The comparisons between all-important combinations of 2 input variables and the achieved statistical parameter values for both training and testing sets of data for Adrar city are listed in Table 2. Once the highest GPI is achieved for a set of inputs, it is calculated as the most significant combination of inputs to predict the global SR and vice versa.

As observed in Table 2, it is found that the combination of H_0 and T_{min} is selected as the most optimal set of 2 inputs with the highest values of GPI = 3.79 and that was verified by a value of (bold numbers) R = 0.9451, RMSE = 0.5255 kWh/m^2, MPE = 6.35% and MABE = 0.313 kWh/m^2 for the training phase. For the testing phase, results indicated a value of R = 0.9360, RMSE = 0.5728 kWh/m^2, MPE = 6.114% and MABE = 0.296 kWh/m^2. From Table 2, the combination of W_s and V_p is determined as the worst choice to predict the global SR with the smallest values of GPI = −3.98.

Figure 5 shows the estimated global SR values by the developed ANFIS model for both training and testing phases, plotted against the measured values. The comparison between the optimal and least combinations of inputs (i.e., the highest and lowest rank) proves valuable in demonstrating the extent of the difference in prediction accuracy that occurs between the sets of greatest and least relevant of 2 inputs. The comparative values of the global SR models ranking are determined based on the GPI, as depicted in Table 3.

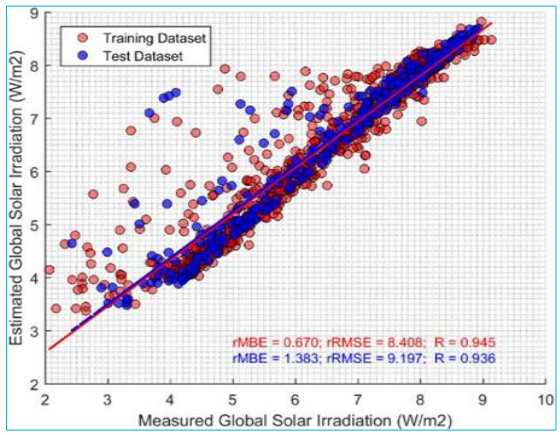

Figure 5. Scatter plot of the examined ANFIS model for the optimal combinations with 2

Table 2. Statistical analysis of the training and testing periods, including the ranking of input parameters for Case 1 (2 inputs)

Models No.	Combination	Training				Testing					
		R	RMSE	MPE	MABE	R	RMSE	MPE	MABE	GPI	Rank
1	H_0, T_{min}	0.9451	0.5255	6.358	0.3133	0.9360	0.5728	6.114	0.2963	3.79	1
2	H_0, T_{max}	0.9342	0.5736	6.926	0.3387	0.9349	0.5788	6.279	0.3028	3.61	2
3	H_0, T_{avg}	0.9280	0.5983	7.254	0.3639	0.9317	0.5922	6.427	0.3132	3.43	5
4	H_0, R_h	0.9280	0.5993	7.190	0.3624	0.9416	0.5490	6.350	0.3122	3.57	3
5	H_0, W_s	0.9271	0.6024	7.231	0.3530	0.9366	0.5719	6.448	0.3158	3.44	4
6	H_0, V_p	0.9278	0.5990	7.257	0.3611	0.9341	0.5815	6.529	0.3209	3.34	6
7	T_{min}, T_{max}	0.8455	0.8588	11.325	0.6293	0.8609	0.8375	9.952	0.5792	−0.67	13
8	T_{min}, T_{avg}	0.8646	0.8062	10.590	0.5858	0.8763	0.7893	8.978	0.5256	0.42	8
9	T_{min}, R_h	0.8527	0.8404	10.972	0.5804	0.8841	0.7669	9.673	0.5092	−0.23	12
10	T_{min}, W_s	0.8036	0.9600	12.994	0.6913	0.8033	0.9709	12.809	0.6750	−3.82	19
11	T_{min}, V_p	0.7700	1.0301	14.211	0.7552	0.8005	0.9689	12.895	0.6762	−3.90	20
12	T_{max}, T_{avg}	0.8188	0.9235	12.108	0.6533	0.8450	0.8804	10.943	0.6155	−1.76	14
13	T_{max}, R_h	0.8573	0.8289	10.746	0.5700	0.8947	0.7415	9.248	0.4949	0.24	9
14	T_{max}, W_s	0.8156	0.9310	12.260	0.6570	0.8394	0.8921	11.025	0.6212	−1.86	15
15	T_{max}, V_p	0.8166	0.9306	12.491	0.6708	0.8492	0.8582	11.118	0.5948	−1.89	16
16	T_{avg}, R_h	0.8544	0.8366	10.911	0.5784	0.8853	0.7625	9.443	0.4954	0.02	11
17	T_{avg}, W_s	0.8077	0.9487	12.729	0.6792	0.8299	0.9122	11.653	0.6408	−2.54	17
18	T_{avg}, V_p	0.8129	0.9387	12.746	0.6971	0.8323	0.8973	11.850	0.6256	−2.71	18

19	R_h, W_s	0.8655	0.8050	10.286	0.5407	0.9017	0.7112	8.838	0.4737	0.71	7
20	R_h, V_p	0.8562	0.8315	10.792	0.5723	0.8949	0.7367	9.366	0.4907	0.14	10
21	W_s, V_p	0.7407	1.0807	14.842	0.7778	0.8182	0.9476	13.014	0.6717	−3.98	21

Note: The GPI is a relative and unbounded metric; higher values reflect superior statistical performance and improved modeling quality; Correlation Coefficient (R), Root Mean Square Error (RMSE), Mean Percentage Error (MPE), Mean Absolute Bias Error (MABE), Global Performance Indicator (GPI).

Table 3. Statistical analysis of the training and testing periods, including the ranking of input parameters for Case 2 (3 inputs)

Models		Training				Testing					
No.	Combination	R	RMSE	MPE	MABE	R	RMSE	MPE	MABE	GPI	Rank
1	H_0, T_{min}, T_{max}	0.9576	0.4630	5.548	0.2860	0.9547	0.4818	5.313	0.2763	4.127	2
2	H_0, T_{min}, T_{avg}	0.9589	0.4558	5.540	0.2866	0.9558	0.4769	5.322	0.2711	4.129	1
3	H_0, T_{min}, R_h	0.9527	0.4882	5.972	0.3055	0.9436	0.5405	6.029	0.2962	3.322	4
4	H_0, T_{min}, W_s	0.9463	0.5198	6.202	0.3032	0.9377	0.5678	6.014	0.2921	3.308	5
5	H_0, T_{min}, V_p	0.9463	0.5195	6.278	0.3119	0.9357	0.5727	6.090	0.2982	3.218	6
6	H_0, T_{max}, T_{avg}	0.9546	0.4782	5.650	0.2804	0.9441	0.5326	5.919	0.3018	3.434	3
7	H_0, T_{max}, R_h	0.9307	0.5879	7.052	0.3509	0.9355	0.5763	6.425	0.3115	2.867	12
8	H_0, T_{max}, W_s	0.9446	0.5276	6.331	0.3134	0.9335	0.5841	6.108	0.2929	3.193	7
9	H_0, T_{max}, V_p	0.9284	0.5963	7.137	0.3515	0.9287	0.6037	6.477	0.3146	2.778	14
10	H_0, T_{avg}, R_h	0.9376	0.5589	6.662	0.3233	0.9373	0.5695	6.234	0.3022	3.075	8
11	H_0, T_{avg}, W_s	0.9291	0.5941	7.104	0.3513	0.9278	0.6074	6.410	0.3106	2.843	13
12	H_0, T_{avg}, V_p	0.9348	0.5701	6.850	0.3388	0.9312	0.5942	6.362	0.3059	2.913	10
13	H_0, R_h, W_s	0.9346	0.5718	6.917	0.3487	0.9409	0.5514	6.423	0.3212	2.889	11
14	H_0, R_h, V_p	0.9347	0.5708	6.786	0.3343	0.9392	0.5609	6.308	0.3080	3.007	9
15	H_0, W_s, V_p	0.9274	0.6014	7.181	0.3584	0.9316	0.5907	6.526	0.3209	2.738	15
16	T_{min}, T_{max}, T_{avg}	0.8723	0.7869	10.124	0.5296	0.8873	0.7578	8.970	0.5162	−0.113	22
17	T_{min}, T_{max}, R_h	0.8725	0.7867	10.246	0.5586	0.8892	0.7505	9.022	0.5058	−0.145	23
18	T_{min}, T_{max}, W_s	0.8586	0.8234	10.870	0.6024	0.8596	0.8465	9.611	0.5671	−0.921	29
19	T_{min}, T_{max}, V_p	0.8531	0.8377	11.106	0.6078	0.8729	0.7979	9.741	0.5569	−0.979	30
20	T_{min}, T_{avg}, R_h	0.8817	0.7567	9.755	0.5336	0.8955	0.7292	8.630	0.4911	0.289	16
21	T_{min}, T_{avg}, W_s	0.8595	0.8211	10.470	0.5543	0.8739	0.7950	9.122	0.5318	−0.331	24
22	T_{min}, T_{avg}, V_p	0.8719	0.7869	10.068	0.5519	0.8854	0.7595	8.940	0.5137	−0.083	21
23	T_{min}, R_h, W_s	0.8805	0.7621	10.001	0.5438	0.8963	0.7239	8.947	0.4889	−0.020	19
24	T_{min}, R_h, V_p	0.8611	0.8185	10.516	0.5448	0.8943	0.7330	9.322	0.4871	−0.404	25
25	T_{min}, W_s, V_p	0.7968	0.9709	13.229	0.6937	0.8266	0.9141	12.190	0.6281	−3.662	35
26	T_{max}, T_{avg}, R_h	0.8612	0.8167	10.560	0.5586	0.8891	0.7544	9.308	0.5036	−0.433	26
27	T_{max}, T_{avg}, W_s	0.8250	0.9102	12.246	0.6619	0.8399	0.8935	11.040	0.6350	−2.485	33
28	T_{max}, T_{avg}, V_p	0.8334	0.8892	11.759	0.6440	0.8591	0.8317	10.777	0.5886	−2.094	31
29	T_{max}, R_h, W_s	0.8753	0.7778	9.903	0.5178	0.9040	0.7056	8.718	0.4808	0.244	17
30	T_{max}, R_h, V_p	0.8595	0.8211	10.554	0.5610	0.8943	0.7368	9.340	0.4953	−0.434	27
31	T_{max}, W_s, V_p	0.8212	0.9190	12.219	0.6500	0.8611	0.8353	10.790	0.5847	−2.105	32
32	T_{avg}, R_h, W_s	0.8748	0.7796	9.913	0.5196	0.8945	0.7328	8.929	0.4950	−0.019	18
33	T_{avg}, R_h, V_p	0.8599	0.8223	10.687	0.5723	0.8901	0.7482	9.380	0.4985	−0.493	28
34	T_{avg}, W_s, V_p	0.8120	0.9396	12.533	0.6625	0.8518	0.8572	11.156	0.5929	−2.511	34
35	R_h, W_s, V_p	0.8776	0.7690	9.994	0.5553	0.9065	0.6994	9.026	0.4712	−0.046	20

Note: Correlation Coefficient (R), Root Mean Square Error (RMSE), Mean Percentage Error (MPE), Mean Absolute Bias Error (MABE), Global Performance Indicator (GPI).

3.2 Case 2: Parameter selection for a combination of 3 inputs

To select the optimal combinations of 3 input parameters for the prediction of global SR, 35 different possible combinations of inputs were examined and analyzed. Table 3 displays a comparison of all possible combinations of 3 input variables, along with the corresponding rank values derived from both the training and testing phases. The results demonstrate that the combination of H_0, T_{min}, and T_{avg} is the most optimal sets of 3 inputs with the highest values of GPI = 4.129 and that was validated by a value of R = 0.9589, RMSE = 0.4558 kWh/m^2, MPE = 5.54% and MABE = 0.2866 kWh/m^2 for the training phase and a value of R = 0.9558, RMSE = 0.4769 kWh/m^2, MPE = 5.32% and MABE = 0.271 kWh/m^2 for the testing phase. Furthermore, the combination of T_{min}, W_s, and V_p is determined as the worst choice with the smallest values of GPI = −3.662. The results of the 3-input scenario were slightly better than the 2-input scenario (Figure 6).

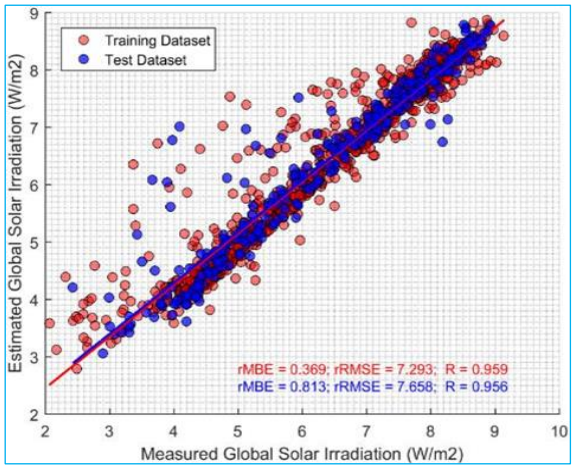

Figure 6. Scatter plot of the examined adaptive neuro-fuzzy inference system (ANFIS) model for the optimal combinations with 3

3.3 Case 3: Parameter selection for a combination of 4 inputs

The third test was conducted to identify the most significant combinations of 4 input parameters. To achieve this, 35 diverse combinations of 4 inputs were analyzed and evaluated. The results for this case are summarized in Table 4. According to the GPI value of 1.264, the most optimal combination is H_0, T_{min}, T_{avg} and R_h, and that was validated by a value of R = 0.9629, RMSE = 0.433 kWh/m^2, MPE = 5.24% and MABE = 0.2719 kWh/m^2 for the training phase and a value of R = 0.954, RMSE = 0.4595 kWh/m^2, MPE = 5.25% and MABE = 0.2684 kWh/m^2 for the testing phase. Moreover, the combination of T_{max}, T_{avg}, W_s and V_p is selected as the worst choice with the smallest values of GPI = 4.247. The results of the 4-input scenario were slightly better than the 3-input scenario (Figure 7).

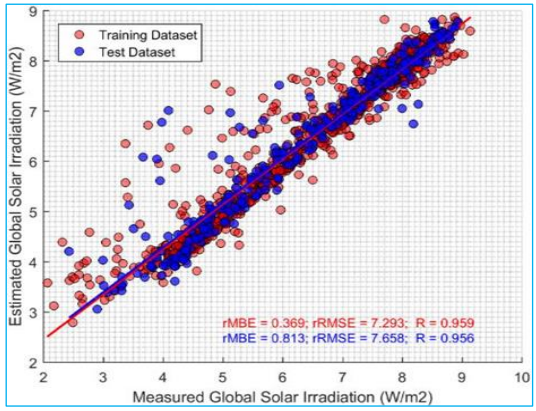

Figure 7. Scatter plot of the examined adaptive neuro-fuzzy inference system (ANFIS) model for the optimal combinations with 4

Table 4. Statistical analysis of the training and testing periods, including the ranking of input parameters for Case 3 (4 inputs)

Models No.		Training				Testing					
	Combination	R	RMSE	MPE	MABE	R	RMSE	MPE	MABE	GPI	Rank
1	H_0, T_{min}, T_{max}, T_{avg}	0.9593	0.4537	5.461	0.2813	0.9550	0.4805	5.293	0.2734	1.198	4
2	H_0, T_{min}, T_{max}, R_h	0.9579	0.4605	5.524	0.2857	0.9562	0.4752	5.438	0.2784	1.055	5
3	H_0, T_{min}, T_{max}, W_s	0.9578	0.4616	5.564	0.2823	0.9532	0.4894	5.508	0.2820	0.965	6
4	H_0, T_{min}, T_{max}, V_p	0.9550	0.4755	5.623	0.2810	0.9518	0.4956	5.511	0.2859	0.950	7
5	H_0, T_{min}, T_{avg}, R_h	0.9629	0.4336	5.245	0.2719	0.9594	0.4595	5.258	0.2684	1.264	1
6	H_0, T_{min}, T_{avg}, W_s	0.9599	0.4497	5.407	0.2808	0.9558	0.4776	5.272	0.2690	1.227	3
7	H_0, T_{min}, T_{avg}, V_p	0.9606	0.4463	5.340	0.2741	0.9573	0.4702	5.250	0.2696	1.258	2
8	H_0, T_{min}, R_h, W_s	0.9564	0.4690	5.652	0.2904	0.9473	0.5199	5.630	0.2768	0.811	8
9	H_0, T_{min}, R_h, V_p	0.9572	0.4649	5.654	0.2927	0.9491	0.5149	5.667	0.2754	0.783	9
10	H_0, T_{min}, W_s, V_p	0.9431	0.5335	6.377	0.3137	0.9373	0.5674	6.021	0.2921	0.347	15
11	H_0, T_{max}, T_{avg}, R_h	0.9540	0.4818	5.870	0.3018	0.9469	0.5208	5.774	0.2926	0.650	11
12	H_0, T_{max}, T_{avg}, W_s	0.9507	0.4975	6.042	0.3103	0.9434	0.5356	5.849	0.2956	0.554	12
13	H_0, T_{max}, T_{avg}, V_p	0.9547	0.4784	5.707	0.2828	0.9446	0.5307	5.684	0.2895	0.731	10
14	H_0, T_{max}, R_h, W_s	0.9364	0.5634	6.724	0.3284	0.9402	0.5552	6.063	0.2945	0.318	17
15	H_0, T_{max}, R_h, V_p	0.9424	0.5371	6.411	0.3187	0.9406	0.5555	6.063	0.2890	0.324	16
16	H_0, T_{max}, W_s, V_p	0.9300	0.5905	7.043	0.3472	0.9271	0.6097	6.394	0.3065	−0.092	20
17	H_0, T_{avg}, R_h, W_s	0.9403	0.5462	6.337	0.3109	0.9420	0.5449	6.033	0.2938	0.361	14
18	H_0, T_{avg}, R_h, V_p	0.9475	0.5138	6.039	0.2994	0.9431	0.5441	5.915	0.2847	0.489	13
19	H_0, T_{avg}, W_s, V_p	0.9304	0.5895	7.011	0.3491	0.9276	0.6076	6.356	0.3061	−0.051	19
20	H_0, R_h, W_s, V_p	0.9348	0.5704	6.760	0.3341	0.9378	0.5664	6.354	0.3098	−0.002	18
21	T_{min}, T_{max}, T_{avg}, R_h	0.8865	0.7421	9.588	0.5275	0.8996	0.7143	8.559	0.4779	−2.561	25
22	T_{min}, T_{max}, T_{avg}, W_s	0.8829	0.7548	9.774	0.5321	0.8879	0.7584	8.749	0.5089	−2.838	27
23	T_{min}, T_{max}, T_{avg}, V_p	0.8664	0.8007	10.566	0.5758	0.8876	0.7519	9.055	0.5131	−3.142	33
24	T_{min}, T_{max}, R_h, W_s	0.8892	0.7361	9.418	0.5049	0.9008	0.7262	8.263	0.4879	−2.286	22
25	T_{min}, T_{max}, R_h, V_p	0.8763	0.7753	9.892	0.5241	0.8957	0.7253	8.852	0.4978	−2.889	28
26	T_{min}, T_{max}, W_s, V_p	0.8615	0.8160	10.512	0.5438	0.8886	0.7548	9.029	0.5190	−3.123	32
27	T_{min}, T_{avg}, R_h, W_s	0.8996	0.7001	8.798	0.4776	0.9043	0.7060	8.000	0.4680	−1.979	21
28	T_{min}, T_{avg}, R_h, V_p	0.8865	0.7428	9.572	0.5210	0.8994	0.7152	8.545	0.4874	−2.558	24
29	T_{min}, T_{avg}, W_s, V_p	0.8860	0.7444	9.505	0.5169	0.9012	0.7181	8.286	0.4839	−2.297	23
30	T_{min}, R_h, W_s, V_p	0.8637	0.8106	10.397	0.5387	0.9034	0.7091	9.096	0.4791	−3.090	31
31	T_{max}, T_{avg}, R_h, W_s	0.8814	0.7581	9.681	0.5341	0.9023	0.7170	8.703	0.4957	−2.723	26
32	T_{max}, T_{avg}, R_h, V_p	0.8645	0.8077	10.607	0.5672	0.8919	0.7411	9.202	0.4963	−3.257	34
33	T_{max}, T_{avg}, W_s, V_p	0.8391	0.8737	11.644	0.6299	0.8726	0.8026	10.049	0.5583	−4.247	35
34	T_{max}, R_h, W_s, V_p	0.8759	0.7737	9.997	0.5458	0.9027	0.7130	8.992	0.4859	−2.998	29
35	T_{avg}, R_h, W_s, V_p	0.8645	0.8084	10.265	0.5335	0.8986	0.7225	9.041	0.4839	−3.058	30

Note: Correlation Coefficient (R), Root Mean Square Error (RMSE), Mean Percentage Error (MPE), Mean Absolute Bias Error (MABE), Global Performance Indicator (GPI).

Table 5. Statistical analysis of the training and testing periods, including the ranking of input parameters for Case 4 (5 inputs)

Models No.		Training				Testing					
	Combination	R	RMSE	MPE	MABE	R	RMSE	MPE	MABE	GPI	Rank
1	H_0, T_{min}, T_{max}, T_{avg}, R_h	0.9556	0.4734	5.612	0.2871	0.9567	0.4729	5.529	0.284	0.15	8
2	H_0, T_{min}, T_{max}, T_{avg}, W_s	0.9567	0.4680	5.657	0.2915	0.9540	0.4866	5.521	0.282	0.15	9
3	H_0, T_{min}, T_{max}, T_{avg}, V_p	0.9571	0.4653	5.611	0.2871	0.9539	0.4854	5.424	0.281	0.24	7

4	H_0, T_{min}, T_{max}, R_h, W_s	0.9617	0.4407	5.265	0.2712	0.9585	0.4611	5.156	0.266	0.56	2
5	H_0, T_{min}, T_{max}, R_h, V_p	0.9600	0.4491	5.442	0.2822	0.9549	0.4807	5.283	0.272	0.40	5
6	H_0, T_{min}, T_{max}, W_s, V_p	0.9587	0.4564	5.500	0.2849	0.9530	0.4905	5.386	0.276	0.28	6
7	H_0, T_{min}, T_{avg}, R_h, W_s	0.9627	0.4346	5.228	0.2699	0.9643	0.4306	4.972	0.255	0.79	1
8	H_0, T_{min}, T_{avg}, R_h, V_p	0.9591	0.4543	5.424	0.2799	0.9570	0.4707	5.253	0.270	0.44	4
9	H_0, T_{min}, T_{avg}, W_s, V_p	0.9624	0.4362	5.287	0.2739	0.9575	0.4691	5.216	0.267	0.49	3
10	H_0, T_{min}, R_h, W_s, V_p	0.9494	0.5054	5.975	0.2962	0.9467	0.5259	5.730	0.275	−0.10	12
11	H_0, T_{max}, T_{avg}, R_h, W_s	0.9570	0.4659	5.666	0.2933	0.9484	0.5130	5.624	0.285	0.01	10
12	H_0, T_{max}, T_{avg}, R_h, V_p	0.9552	0.4750	5.774	0.2945	0.9479	0.5157	5.627	0.288	0.00	11
13	H_0, T_{max}, T_{avg}, W_s, V_p	0.9511	0.4957	6.000	0.3063	0.9425	0.5408	5.873	0.300	−0.29	13
14	H_0, T_{max}, R_h, W_s, V_p	0.9352	0.5690	6.662	0.3245	0.9367	0.5723	6.105	0.292	−0.55	15
15	H_0, T_{avg}, R_h, W_s, V_p	0.9414	0.5423	6.488	0.3184	0.9404	0.5542	6.049	0.292	−0.48	14
16	T_{min}, T_{max}, T_{avg}, R_h, W_s	0.8852	0.7472	9.537	0.5128	0.8985	0.7220	8.396	0.486	−3.23	20
17	T_{min}, T_{max}, T_{avg}, R_h, V_p	0.8891	0.7343	9.322	0.5106	0.9056	0.6949	8.401	0.473	−3.18	18
18	T_{min}, T_{max}, T_{avg}, W_s, V_p	0.8878	0.7380	9.388	0.5097	0.9039	0.7056	8.380	0.486	−3.19	19
19	T_{min}, T_{max}, R_h, W_s, V_p	0.8948	0.7166	9.172	0.4942	0.9132	0.6739	8.146	0.468	−2.89	17
20	T_{min}, T_{avg}, R_h, W_s, V_p	0.9028	0.6897	8.586	0.4614	0.9183	0.6548	7.711	0.447	−2.41	16
21	T_{max}, T_{avg}, R_h, W_s, V_p	0.8699	0.7939	10.180	0.5401	0.9083	0.6946	8.808	0.484	−3.60	21

3.4 Case 4: Parameter selection for a combination of 5 inputs

The final test was performed to identify the optimal combinations of 5 input parameters. 21 different combinations of 5 inputs were examined and analyzed. The results are provided in Table 5. The most optimal combination with the highest values of GPI = 0.79 is H_0, T_{min}, T_{avg}, R_h and W_s and that was validated by a value of R = 0.9627, RMSE = 0.434 kWh/m^2, MPE = 5.22% and MABE = 0.269 kWh/m^2 for the training phase and a value of R = 0.9643, RMSE = 0.4306 kWh/m^2, MPE = 5.22% and MABE = 0.269 kWh/m^2 for the testing phase. In addition, the combination of T_{max}, T_{avg}, W_s and V_p is selected as the worst choice with the smallest values of GPI = −3.60.

The results of the 4-input scenario were slightly better than the 5-input scenario (Figure 8).

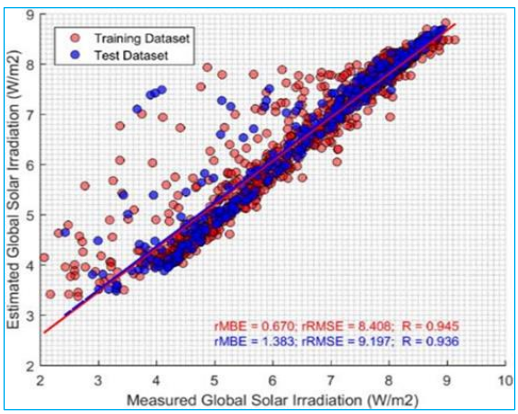

Figure 8. Scatter plot of the examined adaptive neuro-fuzzy inference system (ANFIS) model for the optimal combinations with 5

3.5 Comparing different cases and introducing the optimal combination of inputs

Even though Sections 3.1 to 3.4 identified the most optimal combinations of 2, 3, 4, and 5 inputs for global SR prediction, it is essential to introduce the overall best (or optimal) combination among them. In this current study, the evaluation is based only on the RMSE indicator. The RMSE values (kWh/m^2) during both the training and testing phases for the optimal combinations of parameters with 2, 3, 4 and 5 inputs, as shown in Figure 9. The combination of H_0, T_{min}, T_{avg}, R_h and W_s is the optimum input parameter to predict the daily horizontal global SR in Adrar city using the ANFIS model.

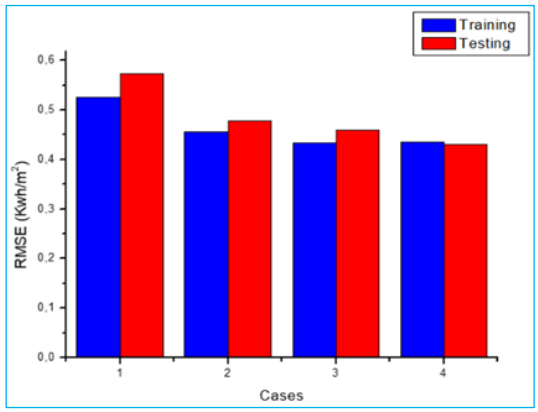

Figure 9. Root Mean Square Error (RMSE) (kWh/m^2) for the most significant combinations of all cases

In general, a model that prioritizes simplicity regarding required inputs is preferred. Using more than 2 inputs in constructing the ANFIS model may not be suitable or applicable. It is evident that among the commonly appropriate input sets for Adrar city, two parameters, T_{min} and H_0, have been identified as the most influential elements.

4. CONCLUSION

Through this work, the ANFIS technique was employed to select the most important parameters to predict daily global SR (H). As a case study, 5 years of measured data from Adrar city were utilized. H_0, T_{max}, T_{avg}, T_{min}, R_h, W_s, and V_p were used as parameter variables. To identify the most optimal combinations of 2, 3, 4 and 5 inputs, we considered and analyzed 21, 35, 35 and 21 possible combinations, respectively. Four statistical indicators (R, RMSE, MPE and MABE) were employed to evaluate the model's performance. For each input combination, the GPI was employed as a reliable benchmark to demonstrate the precision of predicting H. Consequently, this approach was used for identifying the rank values of each input parameter, in order of relevance, from most to least. The obtained results indicated that:

(i) The most optimal combination of H_0 and T_{min} for 2 inputs, H_0, T_{min}, and T_{avg} for 3 inputs, H_0, T_{min}, T_{avg} and R_h for 4 inputs and H_0, T_{min}, T_{avg}, R_h and W_s for 5 inputs.

(ii) An increase in the number of relevant inputs leads to a reduction in error (RMSE), thereby improving prediction accuracy.

(iii) The combination of H_0, T_{min}, T_{avg}, R_h and W_s is the optimum input parameter to predict daily horizontal global SR in Adrar city using the ANFIS model.

The results of this study provide valuable insights into SR patterns in the Algerian Big South and can help guide the development of effective solar energy strategies in the region. Moreover, the ANFIS model developed for Adrar has the potential to be applied to other southern Algerian cities with comparable hyper-arid climates, such as Tamanrasset or Illizi, though some local calibration would be necessary. This demonstrates the model's flexibility while emphasizing the importance of site-specific adjustments to maintain predictive accuracy across different desert environments.

REFERENCES

[1] Abdeljabar, B., Rahmani, L., Mebrouk, B., Kada, B. (2020). Estimating daily diffuse solar radiation using neuro-fuzzy, fuzzy C-means and subtractive clustering: Case study: Adrar, Algeria. In ICIST '20: Proceedings of the 10th International Conference on Information Systems and Technologies, Lecce, Italy, pp. 1-6. https://doi.org/10.1145/3447568.3448516

[2] Pourasl, H.H., Barenji, R.V., Khojastehnezhad, V.M. (2023). Solar energy status in the world: A comprehensive review. Energy Reports, 10: 3474-3493. https://doi.org/10.1016/j.egyr.2023.10.022

[3] Himri, Y., Rehman, S., Mostafaeipour, A., Himri, S., Merzouk, M., Kasbadji Merzouk, N. (2024). Contribution of Renewable Energy in Algeria. In Alternative Energy Resources in the MENA Region, pp. 189-212. https://doi.org/10.1007/698_2022_939

[4] Attya, M., Abo-Seida, O.M., Abdulkader, H.M., Mohammed, A.M. (2025). Advanced solar radiation prediction using combined satellite imagery and tabular data processing. Scientific Reports, 15: 14035. https://doi.org/10.1038/s41598-025-96109-0

[5] Huang, G.H., Li, Z.Q., Li, X., Liang, S.L., Yang, K., Wang, D.D., Zhang, Y. (2019). Estimating surface solar irradiance from satellites: Past, present, and future perspectives. Remote Sensing of Environment, 233: 111371. https://doi.org/10.1016/j.rse.2019.111371

[6] Babahadj, A., Rahmani, L., Bouchouicha, K., Brahim, B., Necaibia, A., Mebrouk, B. (2019). ANFIS technique to estimate daily global solar radiation by day in southern Algeria. In International Conference in Artificial Intelligence in Renewable Energetic Systems, Tipaza, Algeria, pp. 41-50. https://doi.org/10.1007/978-3-030-37207-1_5

[7] Dong, J., Olama, M.M., Kuruganti, T., Melin, A.M., Djouadi, S.M., Zhang, Y., Xue, Y. (2020). Novel stochastic methods to predict short-term solar radiation and photovoltaic power. Renewable Energy, 145: 333-346. https://doi.org/10.1016/j.renene.2019.05.073

[8] Almorox, J., Voyant, C., Bailek, N., Kuriqi, A., Arnaldo, J.A. (2021). Total solar irradiance's effect on the performance of empirical models for estimating global solar radiation: An empirical-based review. Energy, 236: 121486. https://doi.org/10.1016/j.energy.2021.121486

[9] Besharat, F., Dehghan, A.A., Faghih, A.R. (2013). Empirical models for estimating global solar radiation: A review and case study. Renewable and Sustainable Energy Reviews, 21: 798-821. https://doi.org/10.1016/j.rser.2012.12.043

[10] Quej, V.H., Almorox, J., Arnaldo, J.A., Saito, L. (2017). ANFIS, SVM and ANN soft-computing techniques to estimate daily global solar radiation in a warm sub-humid environment. Journal of Atmospheric and Solar-Terrestrial Physics, 155: 62-70. https://doi.org/10.1016/j.jastp.2017.02.002

[11] Lee, S., Lee, K.K., Yoon, H. (2019). Using artificial neural network models for groundwater level forecasting and assessment of the relative impacts of influencing factors. Hydrogeology Journal, 27(2): 567-579. https://doi.org/10.1007/s10040-018-1866-3

[12] Mellit, A., Arab, A.H., Khorissi, N., Salhi, H. (2007). An ANFIS-based forecasting for solar radiation data from sunshine duration and ambient temperature. In 2007 IEEE Power Engineering Society General Meeting, Tampa, FL, USA, pp. 1-6. https://doi.org/10.1109/PES.2007.386131

[13] Sumithira, T.R., Nirmal Kumar, A. (2012). Prediction of monthly global solar radiation using adaptive neuro fuzzy inference system (ANFIS) technique over the State of Tamilnadu (India): A comparative study. Applied Solar Energy, 48(2): 140-145. https://doi.org/10.3103/S0003701X1202020X

[14] Güçlü, Y.S., Yeleğen, M.Ö., Dabanlı, İ., Şişman, E. (2014). Solar irradiation estimations and comparisons by ANFIS, Angström–Prescott and dependency models. Solar Energy, 109: 118-124. https://doi.org/10.1016/j.solener.2014.08.027

[15] Olatomiwa, L., Mekhilef, S., Shamshirband, S., Petković, D. (2015). Adaptive neuro-fuzzy approach for solar radiation prediction in Nigeria. Renewable and Sustainable Energy Reviews, 51: 1784-1791. https://doi.org/10.1016/j.rser.2015.05.068

[16] Mohammadi, K., Shamshirband, S., Petković, D., Khorasanizadeh, H. (2016). Determining the most important variables for diffuse solar radiation prediction using adaptive neuro-fuzzy methodology; case study: City of Kerman, Iran. Renewable and Sustainable Energy Reviews, 53: 1570-1579. https://doi.org/10.1016/j.rser.2015.09.028

[17] Zou, L., Wang, L., Xia, L., Lin, A., Hu, B., Zhu, H. (2017). Prediction and comparison of solar radiation using improved empirical models and adaptive neuro-fuzzy inference systems. Renewable energy, 106: 343-353. https://doi.org/10.1016/j.renene.2017.01.042

[18] Halabi, L.M., Mekhilef, S., Hossain, M. (2018). Performance evaluation of hybrid adaptive neuro-fuzzy inference system models for predicting monthly global solar radiation. Applied Energy, 213: 247-261. https://doi.org/10.1016/j.apenergy.2018.01.035

[19] Alsharif, M.H., Younes, M.K. (2019). Evaluation and forecasting of solar radiation using time series adaptive neuro-fuzzy inference system: Seoul city as a case study. IET Renewable Power Generation, 13(10): 1711-1723. https://doi.org/10.1049/iet-rpg.2018.5709

[20] Tao, H., Ewees, A.A., Al-Sulttani, A.O., Beyaztas, U., et al. (2021). Global solar radiation prediction over North Dakota using air temperature: Development of novel hybrid intelligence model. Energy Reports, 7: 136-157. https://doi.org/10.1016/j.egyr.2020.11.033

[21] Fraihat, H., Almbaideen, A.A., Al-Odienat, A., Al-Naami, B., De Fazio, R., Visconti, P. (2022). Solar radiation forecasting by pearson correlation using LSTM neural network and ANFIS method: Application in the west-central Jordan. Future Internet, 14(3): 79. https://doi.org/10.3390/fi14030079

[22] Geshnigani, F.S., Golabi, M.R., Mirabbasi, R., Tahroudi, M.N. (2023). Daily solar radiation estimation in Belleville station, Illinois, using ensemble artificial intelligence approaches. Engineering Applications of Artificial Intelligence, 120: 105839. https://doi.org/10.1016/j.engappai.2023.105839

[23] Anupong, W., Jweeg, M.J., Alani, S., Al-Kharsan, I.H., Alviz-Meza, A., Cárdenas-Escrocia, Y. (2023). Comparison of wavelet artificial neural network, wavelet support vector machine, and adaptive neuro-fuzzy inference system methods in estimating total solar radiation in Iraq. Energies, 16(2): 985. https://doi.org/10.3390/en16020985

[24] Halima, D., Djelloul, B., Mehdi, G., Camel, T., Ali, B., Bouchra, B. (2024). Solar radiation estimation based on a new combined approach of artificial neural networks (ANN) and genetic algorithms (GA) in South Algeria. Computers, Materials & Continua, 79(3): 1-16. https://doi.org/10.32604/cmc.2024.051002

[25] Nafa, A.Z.M., Obed, A.A., Abid, A.J., Yaqoob, S.J., Bajaj, M., Blazek, V. (2025). Adaptive neuro-fuzzy modeling for real-time solar irradiance prediction using PV module operating parameters. e-Prime-Advances in Electrical Engineering, Electronics and Energy, 14: 101130. https://doi.org/10.1016/j.prime.2025.101130

[26] Salameh, T., Farag, M.M., Hamid, A.K., Hussein, M. (2025). Adaptive neuro-fuzzy inference system for accurate power forecasting for on-grid photovoltaic systems: A case study in Sharjah, UAE. Energy Conversion and Management: X, 26: 100958. https://doi.org/10.1016/j.ecmx.2025.100958

[27] Halima, D., Djelloul, B., Mehdi, G., Camel, T., Ali, B., Bouchra, B. (2024). Solar radiation estimation based on a new combined approach of artificial neural networks (ANN) and genetic algorithms (GA) in South Algeria. Computers, Materials & Continua, 79(3): 4725-4740. https://doi.org/10.32604/cmc.2024.051002

[28] Bouchouicha, K., Razagui, A., Bachari, N.E.I., Aoun, N. (2015). Mapping and geospatial analysis of solar resource in Algeria. International Journal of Energy, Environment and Economics, 23(6): 735-751.

[29] Oulimar, I., Bouchouicha, K., Bailek, N., Bellaoui, M. (2024). Statistical study of global solar radiation in the Algerian desert: A case study of Adrar town. Theoretical and Applied Climatology, 155(4): 3493-3504. https://doi.org/10.1007/s00704-024-04834-9

[30] Kottek, M., Grieser, J., Beck, C., Rudolf, B., Rubel, F. (2006). World map of the Köppen-Geiger climate classification updated. Meteorologische Zeitschrift, 15(3): 259-263. https://doi.org/10.1127/0941-2948/2006/0130

[31] Bailek, N., Bouchouicha, K., Al-Mostafa, Z., El-Shimy, M., Aoun, N., Slimani, A., Al-Shehri, S. (2018). A new empirical model for forecasting the diffuse solar radiation over Sahara in the Algerian Big South. Renewable Energy, 117: 530-537. https://doi.org/10.1016/j.renene.2017.10.081

[32] Jang, J.S. (1993). ANFIS: Adaptive-network-based fuzzy inference system. IEEE Transactions on Systems, Man, and Cybernetics, 23(3): 665-685. https://doi.org/10.1109/21.256541

[33] Moayedi, H., Kalantar, B., Foong, L.K., Tien Bui, D., Motevalli, A. (2019). Application of three metaheuristic techniques in simulation of concrete slump. Applied Sciences, 9(20): 4340. https://doi.org/10.3390/app9204340

[34] Gampa, S.R., Jasthi, K., Goli, P., Das, D., Bansal, R.C. (2020). Grasshopper optimization algorithm based two stage fuzzy multiobjective approach for optimum sizing and placement of distributed generations, shunt capacitors and electric vehicle charging stations. Journal of Energy Storage, 27: 101117. https://doi.org/10.1016/j.est.2019.101117

[35] Khosravi, K., Daggupati, P., Alami, M.T., Awadh, S.M., et al. (2019). Meteorological data mining and hybrid data-intelligence models for reference evaporation simulation: A case study in Iraq. Computers and Electronics in Agriculture, 167: 105041. https://doi.org/10.1016/j.compag.2019.105041

[36] Kumar, A., Kumar, P., Singh, V.K. (2019). Evaluating different machine learning models for runoff and suspended sediment simulation. Water Resources Management, 33(3): 1217-1231. https://doi.org/10.1007/s11269-018-2178-z

[37] Takagi, T., Sugeno, M. (1985). Fuzzy identification of systems and its applications to modeling and control. IEEE Transactions on Systems, Man, and Cybernetics, SMC-15(1): 116-132. https://doi.org/10.1109/TSMC.1985.6313399